COBEM 2021 26th International Congress of Mechanical Engineering
ABCM Associação Brasileira de Engenharia e Ciências Mecânicas
November 22-26, 2021, Virtual Congress, Brazil

COB-2021-0558
Fluid-structure interaction analysis of a flexible wing using the lifting-line theory and the Euler-Bernoulli beam model via a finite element approach

Murilo Caetano da Silva
Felipe Fernandes Liorbano
Ricardo Afonso Angélico
University of São Paulo, São Carlos School of Engineering, Department of Aeronautics Engineering
m.caetano@usp.br, felipe.liorbano@usp.br, raa@sc.usp.br

Abstract. *In the aviation sector, there is a concern over developing new aircraft technologies that are more eco-friendly. Among the advances, the increase of wing aspect-ratio in commercial aircraft and the incorporation of composite materials may lead to slender structures contributing to weight and drag reduction. Furthermore, it also provides aerodynamic surfaces that exhibit higher structural flexibility. This emphasizes the importance of the coupling between aerodynamic and structural models into an aeroelastic one. One of the approaches consists of using a lifting-line based aerodynamic model and an Euler-Bernoulli structural model. Hence, this article aims to develop an aeroelastic model based on the ones mentioned above using a finite element approach for both domains, viz. aerodynamic and structural. The discretization of both problems with the same numeric approach allows describing the circulation and the displacement fields with a polynomial basis. The routines relative to each model were developed separately and implemented in Python using the object-oriented paradigm. An existing Python code implemented to predict the aerodynamic response of finite wings through the Finite Element Method - previously validated - was modified to compute the nodal forces. These will be used in the structural code to calculate displacements and rotations. On the other hand, structural displacements affect the wing aerodynamic behavior, producing new forces and moments that will deform the structure again. This iterative process continues until it reaches a specified tolerance concerning aerodynamic and structural degrees of freedom increments. A fixed-point algorithm is used for the iterative process. The techniques mentioned above allow obtaining an interaction between the domains without interpolations, which can be interesting for dynamic analysis. In the end, the developed code will be validated by comparison with available literature data. The implemented model comprises a rectangular wing with span* $b = 9.144\ m$*, chord* $c = 0.3048\ m$*, airfoil NACA 0012 with a lift curve slope of* $a_0 = 6.382\ rad^{-1}$*. The aerodynamic load is applied directly to the wing spar, which has an I-shape (*$I_{xx} = 716.1 \times 10^{-9}\ m^4$*,* $S = 3.952 \times 10^{-3}\ m^2$*), manufactured in 6061 aluminum alloy (*$E = 68.95\ GPa$*). Regarding the flight condition, the speed is* $U_\infty = 91.44\ m/s$ *and the wing is analyzed for an angle of attack of* $\alpha = 6.89\ °$*. The proposed model was compared with literature data and exhibits a maximum wingtip displacement difference of 0.06% of the wing semispan.*

Keywords: *fluid-structure interaction, lifting-line theory, beam theory, finite element method, load distribution*

1. INTRODUCTION

High aspect-ratio wings tend to increase aerodynamic efficiency and reduce induced drag, thereby improving the performance and reducing greenhouse gases (Nguyen, 2010). Because of its high aspect-ratio and constituent materials, these wings can present significant structural flexibility, which must be considered in the evaluation of the aircraft performance (Chang *et al.*, 2008; Nguyen and Ting, 2018; Nguyen *et al.*, 2017). For instance, High-Altitude Long Endurance (HALE) vehicles have a high aspect-ratio, and therefore, they are submitted to large structural displacements during usual load conditions (approximately 25% of the wing semispan) and present geometrical nonlinear behavior (Su and Cesnik, 2010). Moreover, the large displacements can change stiffness and dynamic responses of the wing, and therefore, leading to a failure in linear theory to correctly analyse its deformation (Patil *et al.*, 1999).

The structural displacement changes the distribution of the aerodynamic loads, which influences the displacement field. Therefore, there is a coupling between structural and aerodynamic models when considering wings as flexible bodies. Hence, predicting the aeroelastic behavior for systems that display high flexibility is essential since the early stages of the designing process. Low-cost computational tools can simulate the aeroelastic behavior of these systems, reducing design process time and predicting undesirable characteristics. Simplified aerodynamic models based on the lifting-line theory together with one-dimensional beam-like structures may lead to an optimized computational cost to a wing project, being useful for conceptual and preliminary design stages (Cella and Biancolini, 2012).

In this context, the present article presents the coupling of an aerodynamic model for nonplanar wings based on the lifting-line theory with a beam-like structural model. Herein, both models are solved using a finite element approach, which facilitates exchanging information between the models. The proposed model is validated using literature data.

2. AERODYNAMIC MODEL

The aerodynamic model adopted herein is based on the Lifting-Line Theory proposed by Prandtl (1923) and was modified to take nonplanar wing effects into account. In this model, the lifting surface is represented by the combination of horseshoe vortices positioned in its quarter chord locus (Houghton and Carpenter, 2003), which allows obtaining the spanwise lift distribution. An unswept nonplanar wing is considered herein as depicted in Fig. 1, positioned in a Cartesian coordinate system with unit vectors $\hat{\mathbf{i}}$, $\hat{\mathbf{j}}$ and $\hat{\mathbf{k}}$ associated with x, y and z axes, respectively. The position of the quarter chord locus is given by $z = f(y)$ for $y \in [-b/2, b/2]$ and it belongs to the yz plane, with $\hat{n}$ as its normal direction and $\hat{t}$ as its tangential direction. The wing has span b, area S, is subjected to an angle of attack α, and its wake is parallel to the xy plane. Freestream flow has density ρ_∞ and speed U_∞ parallel to the xz plane.

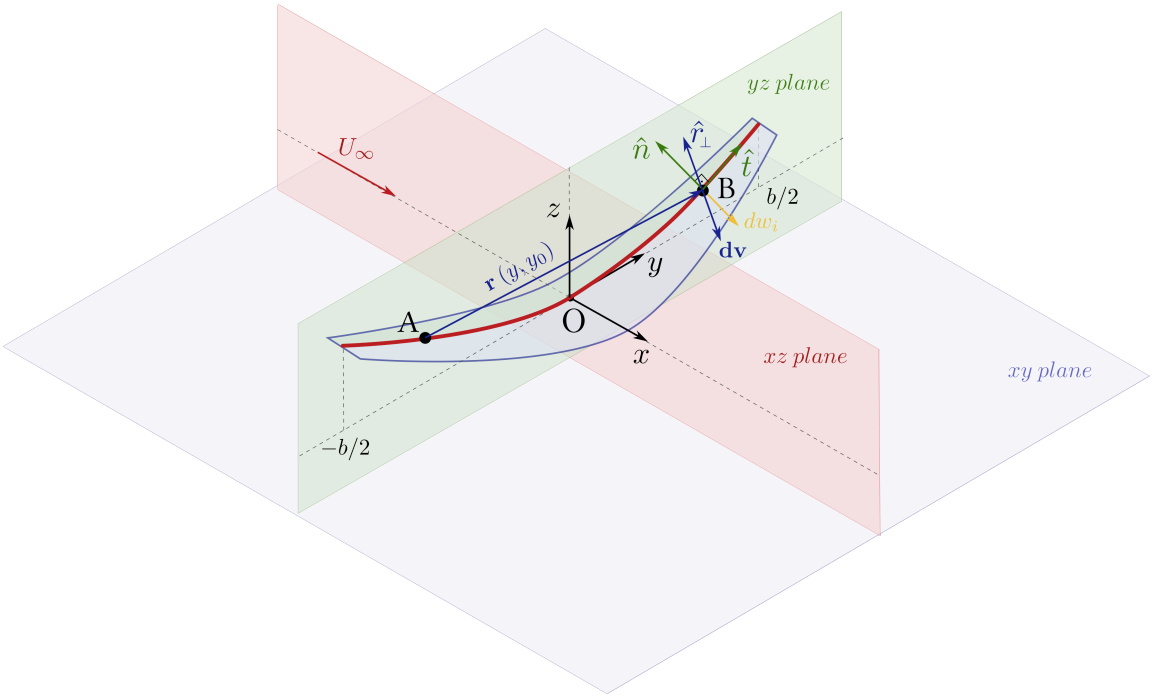

Figure 1. Lifting-line model for an unswept nonplanar wing.

According to Biot-Savart law, an infinitesimal velocity $\mathbf{dv}$ at point B, located at $(0, y, f(y))$, is induced by an infinitesimal vortex filament $d\Gamma$ at point A, located at $(0, y_0, f(y_0))$ (Fig. 1). The induced velocity $\mathbf{dv}$ is parallel to the $r_\perp$ direction, in which r is the vector from A to B. A mathematical expression for $\mathbf{dv}$ may be found by applying the same aforementioned law for this semi-infinite vortex system.

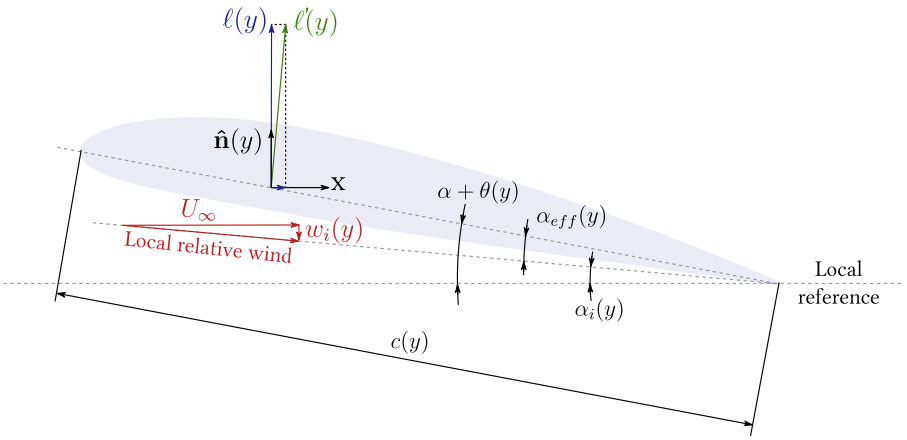

Figure 2. Downwash effect on a wing section.

An infinitesimal downwash dw_i can be found by projecting $\mathbf{dv}$ on the $\hat{\mathbf{n}}$ direction. As the induced velocity at an arbitrary point can be obtained by adding the contributions of each spanwise vortex filament, the total downwash $w_i(y)$ acting on each section can be described as:

$$w_i(y) = -\frac{1}{4\pi}\left[1 + f'(y)^2\right]^{-1/2} \int_{-b/2}^{b/2} \frac{[f(y) - f(y_0)]f'(y) + (y - y_0)}{(y - y_0)^2 + [f(y) - f(y_0)]^2} \frac{d\Gamma}{dy_0}\, dy_0 \tag{1}$$

This integral exists only in a Cauchy sense, as proposed by Mangler (1951), Kythe and Puri (2011) and Mandal and Chakrabarti (2016), and it is noticeable that downwash reduces the effective angle of attack of a wing section, as shown in Fig. 2. This model assumes that local lift $\ell(y)$ varies linearly with the effective angle of attack $\alpha_{eff}(y)$ for each section. The angle $\alpha_{eff}(y)$ may be defined as $\alpha_{eff}(y) = \alpha + \theta(y) - \alpha_i(y)$, in which $\theta(y)$ denotes the spanwise geometric torsion distribution and α_i the induced angle of attack. The angle α_i is defined as $\alpha_i = \tan^{-1}(-w_i/U_\infty) \approx -w_i/U_\infty$, considering that the downwash velocity magnitude is small when compared to the freestream speed. Therefore, the two-dimensional lift coefficient C_ℓ can be mathematically described as:

$$C_\ell(y) = a_0(y)[\alpha_{eff}(y) - \alpha_{L=0}(y)] = a_0(y)\left[\alpha + \theta(y) + \frac{w_i(y)}{U_\infty} - \alpha_{L=0}(y)\right] \tag{2}$$

in which a_0 denotes the airfoil lift curve slope and $\alpha_{L=0}(y)$, the airfoil angle of zero lift.

Figure 2 also reveals that the local relative wind may be approximated by the freestream flow, and it was assumed that $\ell(y) = \ell'(y)\cos\alpha_i \approx \ell'(y)$. With these two informations, the lift per unit span can be related with the sectional lift coefficient as $\ell(y) = (1/2)\rho_\infty U_\infty^2\, c(y)\, C_\ell(y)$, in which $c(y)$ is the section chord. Nonetheless, $\ell(y)$ may also be expressed as $\ell(y) = \rho_\infty U_\infty \Gamma(y)$ by using Kutta-Jouwkowsky theorem (Houghton and Carpenter, 2003), in which $\Gamma(y)$ is the sectional circulation. Therefore, the sectional lift coefficient is given as $C_\ell = 2\Gamma(y)/U_\infty c(y)$ and introduced in Eq. 2, resulting in:

$$\frac{2\Gamma(y)}{U_\infty c(y)} = a_0(y)\left[\alpha + \theta(y) + \frac{w_i(y)}{U_\infty} - \alpha_{L=0}(y)\right] \tag{3}$$

Equation 1 may be introduced in Eq. 3, resulting in the general lifting-line equation for unswept nonplanar wings:

$$\frac{2}{U_\infty c(y) a_0(y)}\Gamma(y) = \alpha + \theta(y) - \alpha_{L=0}(y) - \frac{1}{4\pi U_\infty}\left[1 + f'(y)^2\right]^{-1/2} \int_{-b/2}^{b/2} \frac{[f(y) - f(y_0)]f'(y) + (y - y_0)}{(y - y_0)^2 + [f(y) - f(y_0)]^2} \frac{d\Gamma}{dy_0} dy_0 \tag{4}$$

where $\Gamma(y)$ is the unknown variable. Equation 4 may be rewritten using auxiliary functions $\mathcal{G}(y)$, $\mathcal{H}(y)$, $\mathcal{K}(y)$ as:

$$\mathcal{G}(y)\Gamma(y) - \int_{-b/2}^{b/2} \mathcal{K}(y, y_0) \frac{d\Gamma}{dy_0}\, dy_0 - \mathcal{H}(y) = 0 \tag{5}$$

which corresponds to a second kind Fredholm integro-differential equation (Mandal and Chakrabarti, 2016). The auxiliary functions in Eq. 5 are defined as:

$$\mathcal{G}(y) = \frac{8\pi}{a_0(y)c(y)} \sqrt{1 + f'(y)^2} \tag{6}$$

$$\mathcal{H}(y) = 4\pi U_\infty [\alpha + \theta(y) - \alpha_{L=0}(y)] \sqrt{1 + f'(y)^2} \tag{7}$$

$$\mathcal{K}(y) = \frac{[f(y) - f(y_0)]f'(y) + (y - y_0)}{(y - y_0)^2 + [f(y) - f(y_0)]^2} \tag{8}$$

and they depend solely on wing geometry, airfoil properties and flow parameters.

Equation 5 describes the general lifting-line equation in its strong formulation. For the purpose of applying the Finite Element Method, the equation is rewritten in its weak formulation by using an arbitrary continuous weight function $w(y)$, homogeneous on the essential boundary conditions. Thus, the weighted-residual statement is written as:

$$\int_\Omega w(y) \left[\mathcal{G}(y)\Gamma(y) - \int_\Omega \mathcal{K}(y, y_0) \frac{d\Gamma}{dy_0}\, dy_0\right] dy = \int_\Omega w(y)\mathcal{H}(y)\, dy \tag{9}$$

where $\Omega = [-b/2, b/2]$ is the domain that represents the wingspan. This Ω domain is split into n subdomains Ω_e for $e = 1, ..., n$ called finite elements, in which $\Omega_1 \cup \Omega_2 \cup ... \cup \Omega_e \cup ... \cup \Omega_n = \Omega$ and $\Omega_1 \cap \Omega_2 \cap ... \cap \Omega_e \cap ... \cap \Omega_n = \emptyset$ (Zienkiewicz *et al.*, 2000). Equation 9 is then rewritten as:

$$\sum_{e=1}^{n} \int_{\Omega_e} w^{(e)}(y) \left[\mathcal{G}^{(e)}(y)\Gamma^{(e)}(y) - \sum_{k=1}^{n} \fint_{\Omega_k} \mathcal{K}(y, y_0) \frac{d\Gamma^{(k)}}{dy_0} dy_0 \right] dy = \sum_{e=1}^{n} \int_{\Omega_e} w^{(e)}(y)\, \mathcal{H}^{(e)}(y)\, dy \tag{10}$$

The physical interpretation of the inner integral in Eq. 10 is that it represents the sum of the aerodynamic influence of all the subdomain Ω_k acting in subdomain Ω_e.

The approximate solution is obtained by writing both weight and trial functions as linear combinations of p orthogonal shape functions denoted by $\mathbf{N_\Gamma}^{(e)}(y) = [N_{\Gamma_1}(y), N_{\Gamma_2}(y), ..., N_{\Gamma_p}(y)]$. The gamma subscript distinguishes these shape functions from those used in the structural model, which will be presented later on. Hence, $w^{(e)}(y)$ and $\Gamma^{(e)}(y)$ are rewritten as:

$$\Gamma^{(e)}(y) = \mathbf{N_\Gamma}^{(e)}(y)\ \mathbf{d_\Gamma}^{(e)} \quad \text{and} \quad w^{(e)}(y) = \mathbf{N_\Gamma}^{(e)}(y)\ \mathbf{d_w}^{(e)} \tag{11}$$

in which $\mathbf{d_\Gamma}^{(e)}$ represents the nodal values of the trial function and $\mathbf{d_w}^{(e)}$ the nodal values of the weight function. In this paper, $\mathbf{N_\Gamma}^{(e)}(y)$ is particularized to a linear-shaped function and will be denoted as LL2. Note that both functions are approximated by the same orthogonal basis functions, as proposed by the Galerkin Method (Zienkiewicz *et al.*, 2000). Introducing Eq. 11 into Eq. 10 results in:

$$\sum_{e=1}^{n} \int_{\Omega_e} \mathbf{d_w}^{(e)^T} \mathbf{N_\Gamma}^{(e)^T} \left[\mathcal{G}^{(e)}(y) \mathbf{N_\Gamma}^{(e)} \mathbf{d_\Gamma}^{(e)} - \sum_{k=1}^{n} \fint_{\Omega_k} \mathcal{K}(y, y_0) \frac{d\mathbf{N_\Gamma}^{(k)}}{dy_0} \mathbf{d_\Gamma}^{(k)}\, dy_0 \right] dy = \sum_{e=1}^{n} \int_{\Omega_e} \mathbf{d_w}^{(e)^T} \mathbf{N_\Gamma}^{(e)^T} \mathcal{H}^{(e)}(y)\, dy \tag{12}$$

Local degrees of freedom $\mathbf{d_\Gamma}^{(e)}$ and weights $\mathbf{d_w}^{(e)}$ may then be related to global vectors $\mathbf{d_\Gamma}$ and $\mathbf{d_w}$ by using a local gathering matrix $\mathbf{L}^{(e)}$ and writing:

$$\mathbf{d_\Gamma}^{(e)} = \mathbf{L}^{(e)} \mathbf{d_\Gamma} \quad \text{and} \quad \mathbf{d_w}^{(e)} = \mathbf{L}^{(e)} \mathbf{d_w} \tag{13}$$

By introducing Eq. 13 into Eq. 12, a global system of equations is obtained:

$$\sum_{e=1}^{n} \int_{\Omega_e} \mathbf{d_w}^T \mathbf{L}^{(e)^T} \mathbf{N_\Gamma}^{(e)^T} \left[\mathcal{G}^{(e)}(y) \mathbf{N_\Gamma}^{(e)} \mathbf{L}^{(e)} \mathbf{d_\Gamma} - \sum_{k=1}^{n} \fint_{\Omega_k} \mathcal{K}(y, y_0) \frac{d\mathbf{N_\Gamma}^{(k)}}{dy_0} \mathbf{L}^{(k)} \mathbf{d_\Gamma}\, dy_0 \right] dy = \sum_{e=1}^{n} \int_{\Omega_e} \mathbf{d_w}^T \mathbf{L}^{(e)^T} \mathbf{N_\Gamma}^{(e)^T} \mathcal{H}^{(e)}(y)\, dy \tag{14}$$

and as $\mathbf{d_w}$ may be any function, this system may be rewritten as:

$$(\mathbf{M_\Gamma} + \mathbf{K_\Gamma})\, \mathbf{d_\Gamma} = \mathbf{f_\Gamma} \tag{15}$$

in which:

$$\mathbf{M_\Gamma} = \sum_{e=1}^{n} \mathbf{L}^{(e)^T} \mathbf{M_\Gamma}^{(e)} \mathbf{L}^{(e)} = \sum_{e=1}^{n} \mathbf{L}^{(e)^T} \left[\int_{\Omega_e} \mathbf{N_\Gamma}^{(e)^T} \mathcal{G}(y) \mathbf{N_\Gamma}^{(e)} dy \right] \mathbf{L}^{(e)} \tag{16}$$

$$\mathbf{K_\Gamma} = -\sum_{e=1}^{n} \sum_{k=1}^{n} \mathbf{L}^{(e)^T} \mathbf{K_\Gamma}^{(e,k)} \mathbf{L}^{(k)} = -\sum_{e=1}^{n} \sum_{k=1}^{n} \mathbf{L}^{(e)^T} \left[\int_{\Omega_e} \fint_{\Omega_k} \mathbf{N_\Gamma}^{(e)^T} \mathcal{K}(y, y_0) \frac{d\mathbf{N}^{(k)}}{dy_0} dy_0\, dy \right] \mathbf{L}^{(k)} \tag{17}$$

$$\mathbf{f_\Gamma} = \sum_{e=1}^{n} \mathbf{L}^{(e)^T} \mathbf{f_\Gamma}^{(e)} = \sum_{e=1}^{n} \mathbf{L}^{(e)^T} \int_{\Omega_e} \mathbf{N_\Gamma}^{(e)^T} \mathcal{H}^{(e)}(y)\, dy \tag{18}$$

The system of equations presented in Eq. 1 was implemented in Python, and solving it leads to the description of the distribution of circulation $\Gamma(y)$. This distribution, in turn, allows calculating aerodynamic variables of interest, such as the downwash distribution $w(y)$, lift coefficient C_L, and induced drag coefficient C_{D_i}.

3. STRUCTURAL MODEL

For the structural model, the wing is idealized as an Euler-Bernoulli beam. The finite element formulation for this kind of structural element may be written using a variational approach. For that purpose, the beam total potential energy is given by Craig Jr and Kurdila (2006) as:

$$\Pi = \frac{1}{2}\int_{\Omega} EI_{xx}\left(\frac{d^2u_z}{dy^2}\right)^2 dy - \int_{\Omega} q_z\, u_z\, dy \tag{19}$$

where E is the Young modulus, I_{xx} is the beam second moment of area with respect to the x axis, u_z is the beam displacement with respect to the z axis and q_z denotes the distributed transverse load applied perpendicularly to the beam element as shown in Fig. 3(b). Note that the domain Ω is the same as in the aerodynamic model, i.e., $\Omega = [-b/2, b/2]$ composed only by two-node elements. This domain is also partitioned in n subdomains Ω_e called finite elements that satisfty the relations $\Omega_1 \cup \Omega_2 \cup ... \cup \Omega_e \cup ... \cup \Omega_n = \Omega$ and $\Omega_1 \cap \Omega_2 \cap ... \cap \Omega_e \cap ... \cap \Omega_n = \emptyset$. Therefore, Eq. 19 may be rewritten as:

$$\Pi = \frac{1}{2}\sum_{e=1}^{n}\int_{\Omega_e} (EI_{xx})^{(e)}\left(\frac{d^2u_z^{(e)}}{dy^2}\right)^2 dy - \sum_{e=1}^{n}\int_{\Omega_e} q_z^{(e)}\, u_z^{(e)}\, dy \tag{20}$$

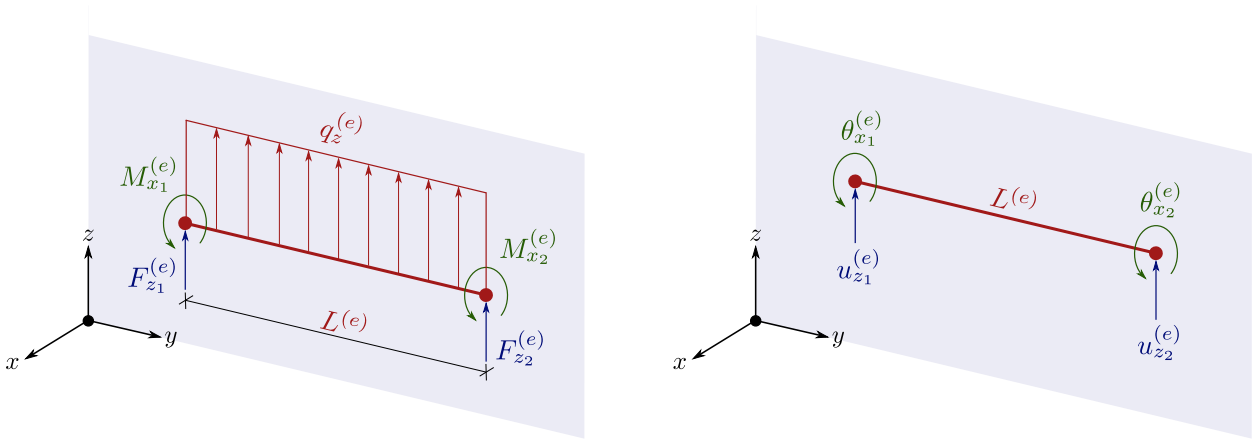

(a) (b)

Figure 3. Finite element used in the structural model: (a) point and distributed loads and moments and (b) structural degrees of freedom.

Considering a finite element Ω_e, the $u_z^{(e)}$ displacement and its second derivative $d^2u_z^{(e)}/dy^2$ may be approximated by:

$$u_z^{(e)}(y) = \mathbf{N_u}^{(e)}\mathbf{d_u}^{(e)} \quad \text{and} \quad \frac{d^2u_z^{(e)}}{dy^2} = \mathbf{B_u}^{(e)}\mathbf{d_u}^{(e)} \tag{21}$$

in which $\mathbf{N_u}^{(e)}$ denotes the q orthogonal shape functions described by $\mathbf{N_u}^{(e)} = [N_{u_1}(y), N_{u_2}(y), ..., N_{u_q}]$ used to approximate the solution, $\mathbf{B_u}^{(e)} = d^2\mathbf{N_u}^{(e)}/dy^2$ and $\mathbf{d_u}^{(e)}$ denotes the vector that contains the degrees of freedom of the beam element, i.e., $\mathbf{d_u}^{(e)} = [u_{z_1} \quad \theta_{x_1} \quad u_{z_2} \quad \theta_{x_2}]^T$, accordingly to Figure 3. In this paper, Hermitian cubic polynomials are used to describe $\mathbf{N_u}^{(e)}$ (Fish and Belytschko, 2007), and the u subscript denotes the difference between these shape functions and those used in the aerodynamic model.

Introducing Eq. 21 in Eq. 20 leads to:

$$\Pi = \frac{1}{2}\sum_{e=1}^{n_e}\mathbf{d_u}^{(e)^T}\left[\int_{\Omega_e}(EI_{xx})^{(e)}\,\mathbf{B_u}^{(e)^T}\mathbf{B_u}^{(e)}\,dy\right]\mathbf{d_u}^{(e)} - \sum_{e=1}^{n_e}\mathbf{d_u}^{(e)^T}\left[\int_{\Omega_e}\mathbf{N_u}^{(e)^T}\,q_z^{(e)}\,dy\right] \tag{22}$$

and this equation may be rewritten as:

$$\Pi = \frac{1}{2}\sum_{e=1}^{n_e}\mathbf{d_u}^{(e)^T}\mathbf{K_u}^{(e)}\,\mathbf{d_u}^{(e)} - \sum_{e=1}^{n_e}\mathbf{d_u}^{(e)^T}\mathbf{f_u}^{(e)} \tag{23}$$

In Eq. 23, $\mathbf{K_u}^{(e)}$ is the stiffness matrix for a finite element Ω_e and $\mathbf{f_u}^{(e)}$ is the equivalent nodal force vector for the same finite element. These matrices are given by:

$$\mathbf{K_u}^{(e)} = \int_{\Omega_e} (EI_{xx})^{(e)}\, \mathbf{B_u}^{(e)^T} \mathbf{B_u}^{(e)}\, dy \tag{24}$$

$$\mathbf{f_u}^{(e)} = \int_{\Omega_e} \mathbf{N_u}^{(e)^T}\, q_z^{(e)}\, dy \tag{25}$$

The four degrees of freedom $\mathbf{d_u}^{(e)}$ of an arbitrary finite element Ω_e may be related to global degrees of freedom $\mathbf{d_u}$ by using a gathering matrix $\mathbf{L}^{(e)}$ and a rotation matrix $\mathbf{T}^{(e)}$ and applying the relation $\mathbf{d_u}^{(e)} = \mathbf{T}^{(e)}\, \mathbf{L}^{(e)}\, \mathbf{d_u}$. With this method, Eq. 23 may be rewritten as:

$$\Pi = \frac{1}{2} \mathbf{d_u}^T \mathbf{K_u}\, \mathbf{d_u} - \mathbf{d_u}^T \mathbf{f_u} \tag{26}$$

in which $\mathbf{K_u}$ is the global stiffness matrix and $\mathbf{f_u}$ is the global equivalent nodal force vector given by:

$$\mathbf{K_u} = \sum_{e=1}^{n_e} \left(\mathbf{L}^{(e)^T} \mathbf{T}^{(e)^T} \mathbf{K_u}^{(e)}\, \mathbf{T}^{(e)}\, \mathbf{L}^{(e)} \right) \tag{27}$$

$$\mathbf{f_u} = \sum_{e=1}^{n_e} \left(\mathbf{L}^{(e)^T} \mathbf{T}^{(e)^T} \mathbf{f_u}^{(e)} \right) \tag{28}$$

with $\mathbf{K_u}^{(e)}$ and $\mathbf{f_u}^{(e)}$ given by Eqs. 24 and 25, respectively. The minimization of the total potential energy with respect to $\mathbf{d_u}$ results in the following system of equations:

$$\mathbf{K_u}\, \mathbf{d_u} = \mathbf{f_u} \tag{29}$$

that represents the structural model used in this article and allows calculating structural displacements and rotations caused by aerodynamic forces.

4. AERODYNAMIC LOADS

The fluid-structure coupling in the presented model is caused by aerodynamic forces and their dependence on the structural shape. As the lift force generated by an airfoil is always perpendicular to the relative flow, the aerodynamic load acting in an arbitrary finite element Ω_e is perpendicular to itself, regardless of its orientation angle concerning the horizontal plane Oxy. However, as this angle changes with structural deformations, new aerodynamic loads must be computed, resulting in an iterative process that continues until an equilibrium wing configuration is reached.

To calculate $\mathbf{f_u}^{(e)} = \left[F_{z_1}^{(e)}, M_{x_1}^{(e)}, F_{z_2}^{(e)}, M_{x_2}^{(e)} \right]$ according to Eqs. 25 and 28, the distributed load $q_z^{(e)}$ must be established for every finite element as a function of the nodal circulation $\Gamma^{(e)}$. Using Kutta-Joukowski theorem (Houghton and Carpenter, 2003), the load distribution function $q_z^{(e)}(y)$ is described for each finite element as:

$$q_z^{(e)}(y) = \rho_\infty\, U_\infty\, \Gamma^{(e)}(y) = \rho_\infty\, U_\infty\, \mathbf{N_\Gamma}^{(e)}(y)\, \mathbf{d_\Gamma}^{(e)} \tag{30}$$

in which $\mathbf{d_\Gamma}^{(e)}$ are the nodal circulation values and $\mathbf{N_\Gamma}^{(e)}(y)$ are the shape functions from the aerodynamic model. Introducing Eq. 30 in Eq. 25 in its matricial form provides means of calculating $\mathbf{f_u}^{(e)}$:

$$\mathbf{f_u}^{(e)} = \rho_\infty\, U_\infty \left(\int_{\Omega_e} \mathbf{N_u}^{(e)^T} \mathbf{N_\Gamma}^{(e)}\, dy \right) \mathbf{d_\Gamma}^{(e)} \tag{31}$$

As the LL2 shape functions were chosen for the aerodynamic model and the Hermitian cubic polynomials were chosen for the structural model, the integration of Eq.31 results in:

$$\mathbf{f_u}^{(e)} = \rho_\infty\, U_\infty\, L^{(e)} \begin{bmatrix} 7/20 & 3/20 \\ L^{(e)}/20 & L^{(e)}/30 \\ 3/20 & 7/20 \\ -L^{(e)}/30 & -L^{(e)}/20 \end{bmatrix} \mathbf{d_\Gamma}^{(e)} \tag{32}$$

With the aerodynamic loads translated to nodal forces and moments, the problem now consists on solving Eqs. (15) and (29) on the variables $\mathbf{d_u}$ and $\mathbf{d_\Gamma}$. Therefore, the model is implemented in Python, in which the *fixed_point* function of the *optimize* module, contained in the *SciPy* library, is used to solve the problem. With this operation, the function is constantly evaluated by using its previous results until a threshold is surpassed. In the present work, this tolerance is given in terms of the L2-norm of displacements and circulation increments and it must be inferior to 10^{-8}.

5. RESULTS

The developed code was applied to a rectangular wing chosen to validate the code with the results presented in Nguyen *et al.* (2017). The wing parameters are described in Tab. 1, its cross-sections are of a NACA 0012 airfoil, and it is at an angle of attack of $\alpha = 6.89°$. As the aerodynamic load presented in Nguyen *et al.* (2017) is elliptical and the wing is rectangular, a geometric twist had to be introduced, guaranteeing that the elliptical aerodynamic load shape will be followed. Knowing that the distribution of the induced angle is constant in an elliptically-loaded wing (Anderson Jr, 2010), it can be found that:

$$\theta(y) = \frac{2L_0}{a_0\, c\, \rho_\infty\, U_\infty^2} \sqrt{1 - \left(\frac{2y}{b}\right)^2} + \frac{L_0}{2b\, \rho_\infty\, U_\infty^2} - \alpha \tag{33}$$

in which L_0 is the maximum value of the lift force located at the wing root, and it takes the value of $L_0 = 1460$ N. Flow parameters are density $\rho_\infty = 1.225$ kg/m^3 and speed $U_\infty = 91.44$ m/s, corresponding to $M_\infty = 0.2687$.

Table 1. Aerodynamic and structural parameters of the wing (Nguyen *et al.*, 2017).

Parameter	Value
b [m]	9.144
c [m]	0.3048
$\mathcal{AR}$ [-]	30
a_0 [rad^{-1}]	6.382
E [GPa]	68.95
I_{xx} [10^{-9} m^4]	716.1
S [10^{-3} m^2]	3.952

A mesh convergence study was conducted to establish the minimum number of elements that verify a difference inferior to 0.1 % concerning the maximum displacement $u_{z_{max}}$ and lift coefficient C_L asymptotes (Fig. 4). This last parameter is given by:

$$C_L = \frac{2}{U_\infty S_w} \int_{-b/2}^{b/2} \Gamma(y)\, \hat{\mathbf{n}} \cdot \hat{\mathbf{k}}\, dy \tag{34}$$

where S_w is the wing area. In the convergence analyses, 13 cases were run by varying the number of elements N from 10 up to 250. With the computed data, it was found that the difference in $u_{z_{max}}$ for $N \geq 60$ is inferior to 0.1 %. Similarly, the variation of the lift coefficient C_L is less than 0.1 % for $N \geq 40$. The results can be further refined by considering a more discretized structure. By taking $N \geq 200$, the code does not exhibit considerable variations anymore. As the calculation time was not drastically increased when using these discretizations, a mesh with 200 finite elements is considered in the following results.

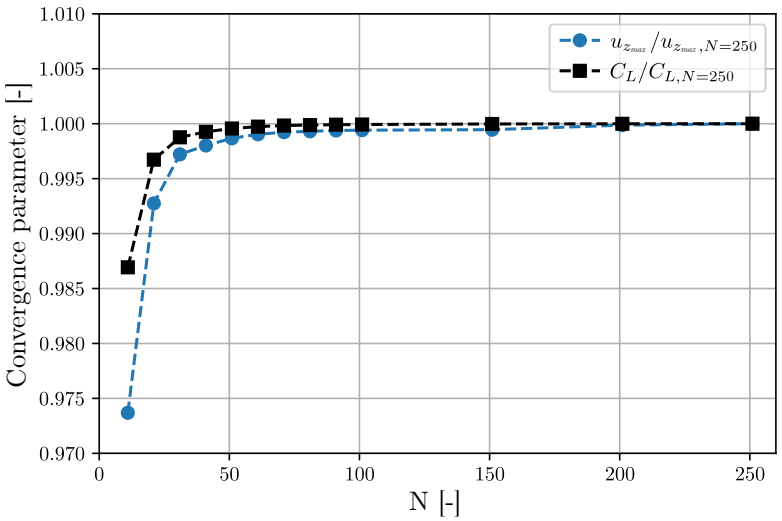

Figure 4. Influence of the mesh discretization on the lift coefficient and the wingtip displacement convergence.

The comparisons of circulation and the wing displacement with respect to the z axis between the proposed model and the literature data are seen in Fig. 5(a) and 5(b). The model presents a good match concerning the circulation distribution and structural displacement. The maximum circulation value is found at the wing root and takes the value of $\Gamma_0 = 13.036$ m^2/s, and the calculated maximum wingtip displacement is $u_{z_{max}} = 982.665$ mm. These results yield maximum absolute differences from the results of Nguyen *et al.* (2017) of 0.00214 m^2/s for the wing root circulation and 2.536 mm for the wingtip displacement.

It is important to remark that the structural model considered herein is linear and not length-preserving, and therefore cannot compute the reduction of the wingspan. Nguyen *et al.* (2017) observed an increase in wing length of 116.6 mm for the linear structural model, whereas the code presented herein exhibited a variation of 117.2 mm in the same parameter, corresponding to 2.56% of the wing semispan, approximately. These measures yield a difference of 0.6 mm between the predicted increase in length by Nguyen *et al.* (2017) and the results contained within this article.

The lift coefficient had a reduction from 0.7342 to 0.7190 when undeformed (planar) and deformed (nonplanar) configurations are considered, respectively. Nguyen *et al.* (2017) predicted that these coefficients would take the values of 0.7338 for the planar wing and 0.7166 for the nonplanar wing. Therefore, the code presented herein also shows a good agreement when calculating C_L, as the differences between the computed coefficients and those provided in the literature were 0.0004 and 0.0024 for the rigid planar and flexible nonplanar configurations, respectively.

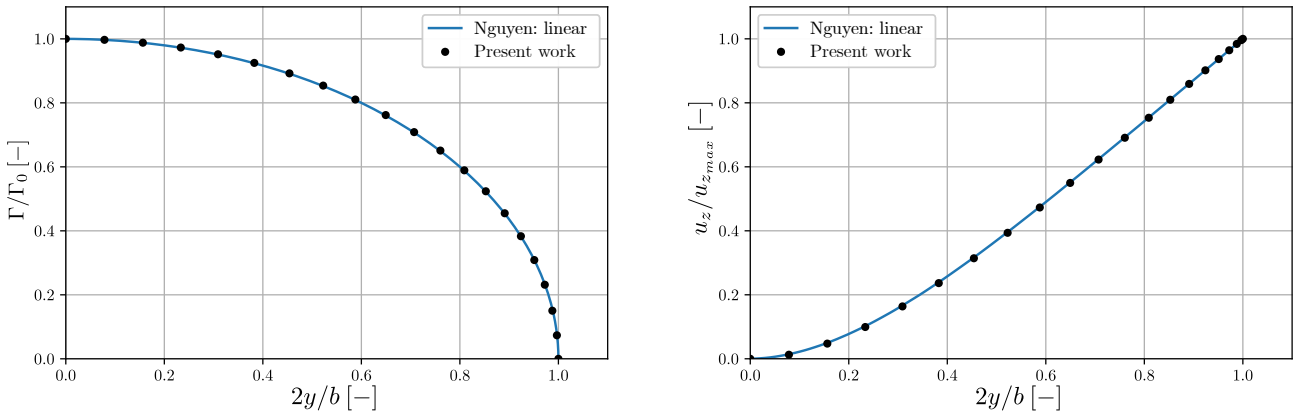

Figure 5. Comparison between the proposed model and Nguyen *et al.* (2017) results: (a) circulation distribution; (b) displacement field.

Due to the approach used to solve the aerodynamic problem, quantities such as induced angle of attack, local lift and local induced drag may also be computed for every element of the model. This is an advantage when compared to other aerodynamic approaches based on a global approximation of the circulation field. The usage of the same numerical strategy for structural and aerodynamic models also facilitates the development of a monolithic approach. Herein, a linear structural model has been used, which is reasonable for wingtip displacements up to 10% of wing semispan. However, it is not length-preserving, leading to a wing with higher span when compared to the nonlinear structural model. Consequently, it presents a better aerodynamic performance, although this effect is not attainable. Using the formulation described in this article, the incorporation of a nonlinear structural model is straightforward and does not change the aerodynamic model described.

6. CONCLUSIONS

This article presents a formulation based on the Finite Element Method that predicts the lift distribution and the displacement field of a flexible wing. The proposed formulation brings the aerodynamic and the structural models closer, since the same approach based on the Finite Element Method is adopted for both problems. The results showed that a mesh with more than 60 elements leads to an error inferior than 0.1% concerning the converged prediction of the maximum wingtip displacement and lift coefficient. Furthermore, the code was validated with the numerical results available in the literature, showing a maximum difference of 2.536 mm for the wingtip displacement, which corresponds to 0.06% of the wing semispan.

Subsequent developments of the present research involve enhancing the formulation to include torsional and wingspan reduction effects and deriving a monolithic model for static aeroelastic analyses, as the usage of the same numerical strategy for the structural and the aerodynamic models facilitates this development. The authors also aim to compare the computational predictions with experimental data, using the results of an experiment with a flexible wing that was conducted by the research group, tested on a wind-tunnel facility, and assisted by non-intrusive measurement techniques.

7. ACKNOWLEDGEMENTS

The authors would like to thank the São Paulo Research Foundation (FAPESP Process 2021/02362-3) and the National Council for Scientific and Technological Development (CNPq Process 141579/2019-6) for the financial support on this project.

8. REFERENCES

Anderson Jr, J.D., 2010. *Fundamentals of aerodynamics*. Tata McGraw-Hill Education.

Cella, U. and Biancolini, M.E., 2012. "Aeroelastic Analysis of Aircraft Wind-Tunnel Model Coupling Structural and Fluid Dynamic Codes". *Journal of Aircraft*, Vol. 49, No. 2, pp. 407–414. ISSN 0021-8669. doi:10.2514/1.c031293.

Chang, C.S., Hodges, D.H. and Patil, M.J., 2008. "Flight dynamics of highly flexible aircraft". *Journal of Aircraft*, Vol. 45, No. 2, pp. 538–545. ISSN 00218669. doi:10.2514/1.30890.

Craig Jr, R.R. and Kurdila, A.J., 2006. *Fundamentals of structural dynamics*. John Wiley & Sons.

Fish, J. and Belytschko, T., 2007. *A First Course in Finite Elements*. Wiley.

Houghton, E.L. and Carpenter, P.W., 2003. *Aerodynamics for engineering students*. Butterworth-Heinemann.

Kythe, P. and Puri, P., 2011. *Computational Methods for Linear Integral Equations*. Birkhäuser Boston.

Mandal, B. and Chakrabarti, A., 2016. *Applied Singular Integral Equations*. CRC Press.

Mangler, K., 1951. *Improper integrals in theoretical aerodynamics*. Royal Aircraft Establishment.

Nguyen, N., 2010. "Nasa innovation fund 2010 project elastically shaped future air vehicle concept".

Nguyen, N.T. and Ting, E., 2018. "Large deflection aeroelasticity and aeroelastic lifting line theory for examination of aerodynamic effects and nonlinear limit cycle oscillations". In *2018 AIAA/ASCE/AHS/ASC Structures, Structural Dynamics, and Materials Conference*. p. 1954.

Nguyen, N.T., Ting, E. and Chaparro, D., 2017. "Nonlinear Large Deflection Theory with Modified Aeroelastic Lifting Line Aerodynamics for a High Aspect Ratio Flexible Wing". In *35th AIAA Applied Aerodynamics Conference*. p. 4219.

Patil, M.J., Hodges, D.H. and Cesnik, C.E., 1999. "Characterizing the effects of geometrical nonlinearities on aeroelastic behavior of high-aspect ratio wings". In *NASA Conference Publication*. NASA, pp. 501–510.

Prandtl, L., 1923. "Applications of modern hydrodynamics to aeronautics". *NACA Technical Report 116*.

Su, W. and Cesnik, C.E., 2010. "Nonlinear aeroelasticity of a very flexible blended-wing-body aircraft". *Journal of Aircraft*, Vol. 47, No. 5, pp. 1539–1553.

Zienkiewicz, O.C., Taylor, R.L., Taylor, R.L. and Taylor, R.L., 2000. *The finite element method: solid mechanics*, Vol. 2. Butterworth-heinemann.

9. RESPONSIBILITY NOTICE

The authors are solely responsible for the printed material included in this paper.